High-Resolution Single-Molecule FRET via DNA eXchange (FRET X)

Filius, Mike; Kim, Sung Hyun; Severins, Ivo; Joo, Chirlmin

DOI
10.1021/acs.nanolett.1c00725

Publication date
2021

Document Version
Final published version

Published in
Nano Letters

NANO LETTERS

pubs.acs.org/NanoLett

Letter

High-Resolution Single-Molecule FRET via DNA eXchange (FRET X)

Mike Filius, Sung Hyun Kim, Ivo Severins, and Chirlmin Joo*

Cite This: *Nano Lett.* 2021, 21, 3295−3301

Read Online

ACCESS | Metrics & More | Article Recommendations | Supporting Information

ABSTRACT: Single-molecule FRET is a versatile tool to study nucleic acids and proteins at the nanometer scale. However, currently, only a couple of FRET pairs can be reliably measured on a single object, which makes it difficult to apply single-molecule FRET for structural analysis of biomolecules. Here, we present an approach that allows for the determination of multiple distances between FRET pairs in a single object. We use programmable, transient binding between short DNA strands to resolve the FRET efficiency of multiple fluorophore pairs. By allowing only a single FRET pair to be formed at a time, we can determine the pair distance with subnanometer precision. The distance between other pairs are determined by sequentially exchanging DNA strands. We name this multiplexing approach FRET X for FRET via DNA eXchange. Our FRET X technology will be a tool for the high-resolution analysis of biomolecules and nanostructures.

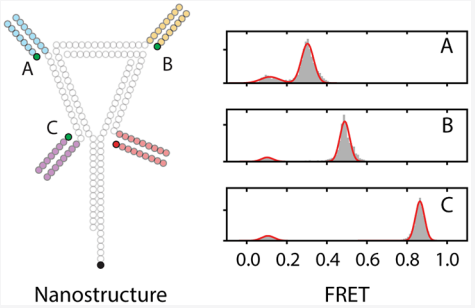

KEYWORDS: *Single-molecule FRET, structural biology, DNA nanotechnology, DNA-PAINT, single-molecule multiplexing*

INTRODUCTION

X-ray crystallography, nuclear magnetic resonance, and cryo-electron microscopy are the gold standard for determining the structure of biomolecules.[1,2] However, minute conformational changes of biomolecules often cannot be observed with these techniques since a certain conformation may be stabilized by the required sample preparation.[3] Single-molecule FRET can be used to determine the structure of molecules, including rare conformations, with subnanometer resolution. However, the use of single-molecule FRET for the analysis of complex molecular structures, for example, protein tertiary structures, has been limited since it requires resolving the FRET efficiency of multiple dye pairs.[4,5] Currently, single-molecule FRET analysis allows us to deal with only one or two FRET pairs in a single measurement.[6,7] Therefore, structural analysis using single-molecule FRET requires the preparation of a protein library consisting of many different combinations of dye locations, rigorous modeling, and simulations following the data acquisition.[8−11]

Single-molecule multiplexing has been demonstrated with photoswitchable fluorophores. In this approach, a molecule of interest is labeled with a single donor and multiple identical acceptor fluorophores. By using photoswitchable acceptor fluorophores, only one of the acceptors is active at a given time.[12] This method, called switchable FRET, allows for the detection of multiple FRET pairs in a single nanoscale object and thereby the determination of structures within and interactions between biomolecules ranging from proteins to DNA. However, the stochastic nature of the photoswitching is one of the main obstacles for the wide adaptation of the method. An alternative way of switching between on and off states of fluorescent probes is by using fluorophores that bind a target only for short period of time, as with point accumulation in nanoscale topography (PAINT).[13−15] For example, fluorophores are attached to short DNA oligos that bind the complementary target strands for several hundreds of milliseconds. This transient binding is central to the super-resolution technique DNA-based point accumulation for imaging in nanoscale topography (DNA-PAINT).[16−19]

Here, we propose a new structural analysis tool that can resolve the FRET efficiency of multiple pairs in a single target molecule. By using programmable, transient binding between short DNA strands, a single FRET pair is formed at any given time allowing for accurate distance determination between the momentarily formed fluorophore pair. By repeating the imaging cycle, we can resolve multiple points of interest (POIs) in a single nanoscale object. We demonstrate the proof of concept of subnanometer resolution single-molecule structural analysis on various DNA nanostructures.

RESULTS

To demonstrate the concept of FRET via DNA strands, we designed an assay where an acceptor (Cy5)-labeled single-stranded (ss) DNA molecule was immobilized on a quartz slide through biotin−streptavidin conjugation (Figure 1A). The measurements yielded a distinct fluorescence signal in

Received: February 22, 2021
Revised: March 10, 2021
Published: March 19, 2021

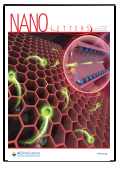

https://doi.org/10.1021/acs.nanolett.1c00725
Nano Lett. 2021, 21, 3295−3301

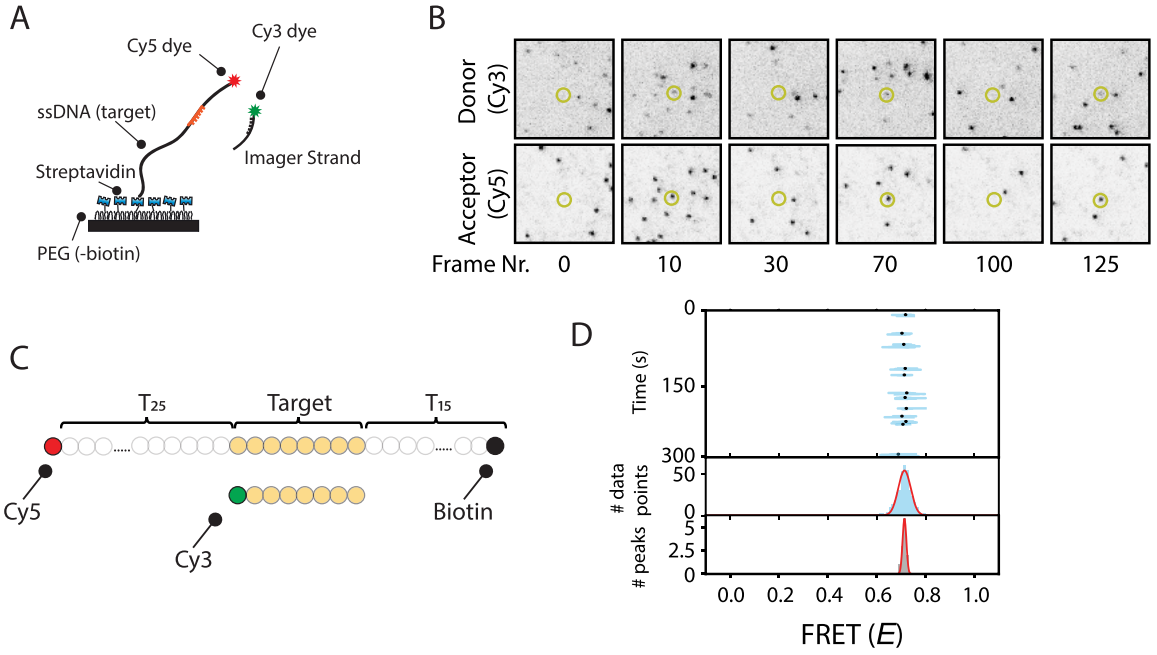

Figure 1. Repetitive binding of short DNA imager strands allows for high detection precision for single-molecule FRET. (A) Schematic representation of the single-molecule FRET assay. An acceptor (Cy5, red star) labeled single-stranded target DNA construct is immobilized on a PEGylated surface through biotin−streptavidin conjugation. Binding of the donor (Cy3, green star) labeled imager strand results in short FRET events and is observed using total internal reflection microscopy. (B) A series of CCD snapshots obtained from a single-molecule movie with 100 ms exposure time. The top row represents the donor channel, and the bottom row represents the acceptor channel. Each dot represents a single molecule. Dynamic binding of the imager strands can be observed over time (highlighted molecule). (C) Schematic representation of the ssDNA constructs. Upon binding of the imager strand, the donor fluorophore is separated from the acceptor by a 25-nt thymine linker. (D) Single-molecule FRET kymograph from a time trace from one single molecule (ROI, highlighted molecule from Figure 1B). The kymograph shows the FRET efficiency for each data point in a binding event (blue lines) and the mean FRET efficiency from all data points per binding event (dots) as a function of time. A FRET histogram that is built from the efficiency for each data point (Figure 1D, middle panel) has a larger standard deviation (0.72 ± 0.05) compared to the standard deviation (0.72 ± 0.01) from a histogram that is built from the mean FRET values per binding events (Figure 1D, bottom panel).

single-molecule total internal refection microscopy images upon binding of a donor-labeled imager strand on the immobilized target strand (Figure 1B). The base sequence and length of the imager strand sequence was chosen such that the binding events between the two DNA strands would have a short dwell-time to allow for frequent replenishment of the imager strand (Figure 1B,C and Supplementary Figure 1A) and thus for the same POI to be probed multiple times.[20] At the same time, the dwell-time was chosen to be long enough, several hundred milliseconds or longer (Supplementary Figure 1), for precise determination of the FRET efficiency.

To visualize the FRET efficiency of each dye pair appearing in a single region of interest (ROI, highlighted as yellow circles in Figure 1B), we built a FRET kymograph (Figure 1D and Supplementary Figure 2A). The kymograph shows the FRET efficiency per data point (Figure 1D, lines) and the mean FRET efficiency from all data points per binding event (Figure 1D, dots). The histograms built with the FRET efficiencies per data points (Figure 1D, middle panel) and per binding event (Figure 1D, bottom panel) show a single FRET population, indicating that imager binding is highly specific to the target site. The ensemble kymograph built from all 363 molecules for this construct shows a similar mean FRET and a standard deviation of 0.71 ± 0.01 (Supplementary Figure 2B).

Analysis of complex biomolecules using single-molecule FRET requires the detection of multiple FRET pairs in a single object. One of the main benefits of FRET via DNA strands over conventional FRET measurements is to use a transiently binding DNA imager strand which can be exchanged by will. Each POI labeled with an orthogonal sequence for the imager binding can be sampled without any crosstalk by means of solution exchange. The absence of crosstalk between the POIs allows for accurate determination of the FRET efficiency of each POI. To illustrate this, we designed a ssDNA construct with two target sequences each of which can interact with a donor-labeled imager strand for 2−3 s giving different FRET efficiencies (Figure 2A and Supplementary Figure 1A,B). The distance between POI B and the acceptor is kept the same for both constructs (35-nt), but the distance for POI A is altered among the constructs (20-nt for Figure 2B,G and 25-nt for Figure 2C,H). When we used the same single imager strand for both POIs separated by a 5-nt spacer (Figure 2B), two FRET peaks were observed (Figure 2D), reporting on the location of each POI. However, when the two POIs were placed with no linker sequence in between (Figure 2C), the FRET histogram became unresolvable (Figure 2E). These results demonstrate that it is not feasible to determine the pair distances of several POIs with high precision using a single imager strand. It is noted that we used an experimental condition to test the resolving power of our approach by structurally compacting the target ssDNA molecule subjected in a buffer of high ionic strength, 100 mM $MgCl_2$ (Supplementary Figure 3).

To achieve higher spatial resolution, we sought to detect the different POIs independently so that the overlapping FRET peaks can be obtained separately and fitted more precisely. As illustrated in Figure 2F, each POI was measured using a unique

https://doi.org/10.1021/acs.nanolett.1c00725
Nano Lett. 2021, 21, 3295−3301

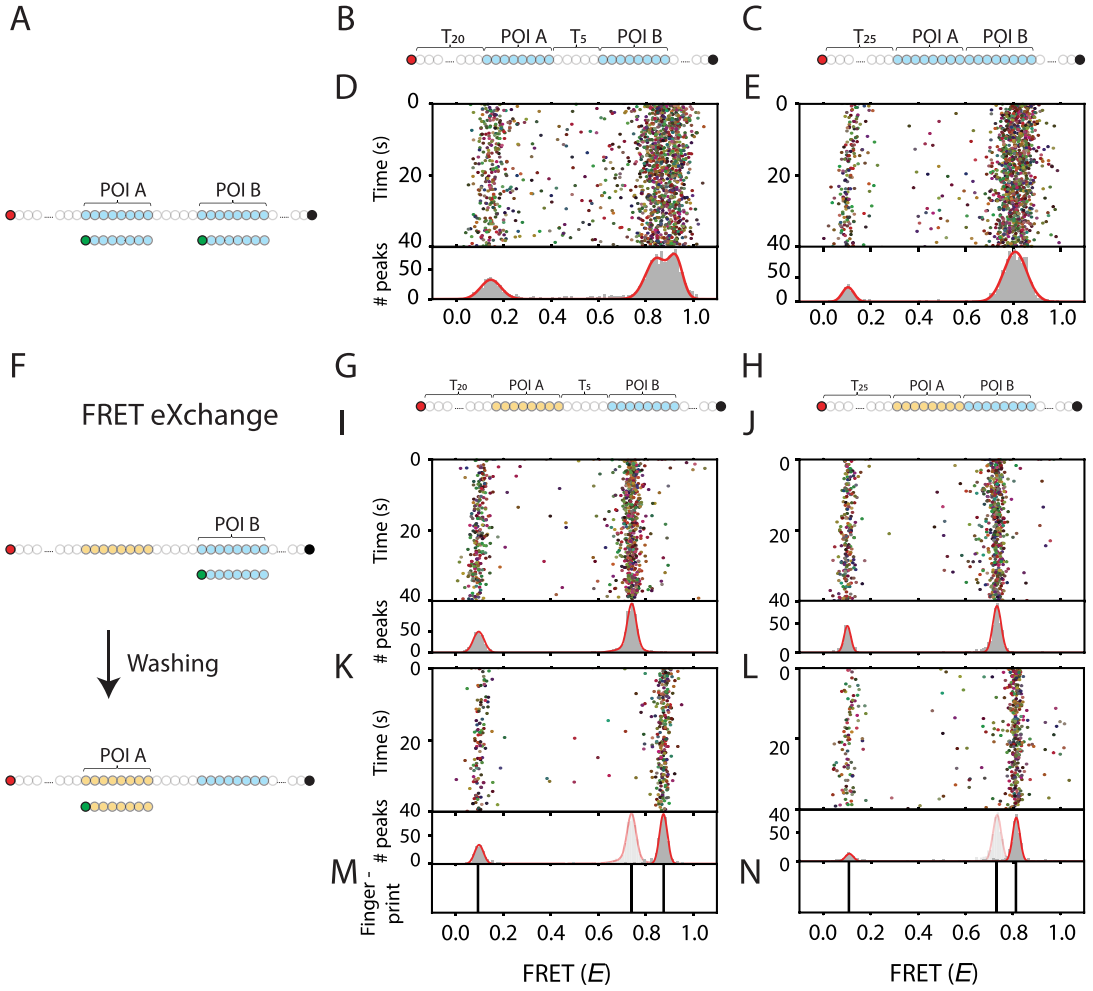

Figure 2. FRET by eXchange of unique imager strands allows for high spatial resolution of multiple POIs in a single nanoscale object. (A) Schematic representation of the single-molecule experiments with two target sequences. A single imager strand is used that can bind to both of the POIs in a target molecule. An acceptor (Cy5, red circle) labeled ssDNA construct contains two POIs. Binding of the donor (Cy3, green circle) labeled imager strand results in either high FRET (when binding to POI A) or mid FRET (when binding to POI B). (B,C) Schematic representation of the target constructs in which two POIs are separated by a 5 thymine linker (panel B) or in which the two POIs are directly connected to each other (panel C). The distance from the acceptor was kept the same for POI B (35-nt) among the two constructs but was altered for POI A (20-nt for panel B and 25-nt for panel C). (D) Single-molecule kymograph of the ssDNA target construct from panel B. Top panel shows the binding events obtained for all molecules in a single field of view. Bottom panel shows a FRET histogram consisting of a donor only peak and two additional FRET peaks reporting on the location of each POI with respect to the acceptor fluorophore. (E) The single-molecule kymograph of the ssDNA target construct from panel C. Using the same imager strand for both POIs does not allow for the detection of the position of both POIs when they are in close proximity. The FRET histogram shows a broad peak at 0.81. (F) Schematic workflow of FRET by eXchange of imager strand (or FRET X). A ssDNA target constructs consists of two POIs with unique DNA binding sequences, allowing us to measure the POIs one at a time. In a first round of detection, the imager strand for POI B (blue circles) is added and imaged for 5 min. Then the microfluidic chamber is washed and an imager strand for POI A (orange circles) is added. (G,H) Schematic representation of the FRET X target constructs in which two unique POI sequences blue circles (POI B) or orange circles (POI A) are separated by a 5-nt thymine linker (panel G) or in which the two POIs are directly adjacent (panel H). (I,J) Single-molecule kymographs for the FRET X for constructs in panel G and H. FRET X imaging allows for the determination of each POI in a separated round. In a first round of FRET X imaging, we observe similar FRET efficiencies for POI B, 0.76 ± 0.05 (panel I) and 0.75 ± 0.01 (panel J). (K,L) Single-molecule kymographs for the second round of FRET X imaging of the constructs in panels G and H. (K) For a construct in which the POIs were separated by a 5-nt thymine linker we observed a FRET efficiency that resulted in a FRET efficiency of 0.87 ± 0.02 for POI A. (L) FRET X allows for the accurate detection of POIs even when they are in closer proximity. We observed a distinct FRET peak in the second FRET X imaging round for POI A of 0.81 ± 0.02 (panel L) and can be clearly separated from POI A (panel J, 0.75 ± 0.02). (M,N) The Gaussian fits of individual histograms for each POI obtained using the FRET X approach allows for the determination of the center of a peak with <0.005 precision. The center of the peaks are plotted in a separate panel, which we name this the FRET fingerprint of a nanoscale object. Mean FRET efficiencies and standard deviation are calculated from three independent experiments.

short DNA imager strand. After recording the binding events for the first POI for several minutes, the imager strand was exchanged by washing the microfluidic chamber and injecting a unique DNA imager strand for the second POI (Figure 2F). This process can be repeated for any number of POIs. We name this method FRET X for FRET via DNA eXchange.

To demonstrate the concept of FRET X, we measured POIs separated by a 5-nt thymine (Figure 2G) linker and POIs in closer proximity with no linker in between (Figure 2H) using two unique imager strands. In case of the 5-nt linker, in the first round of FRET X detection we determined the FRET peak to be at 0.76 for POI B (Figure 2I). In the second round

https://doi.org/10.1021/acs.nanolett.1c00725
Nano Lett. 2021, 21, 3295−3301

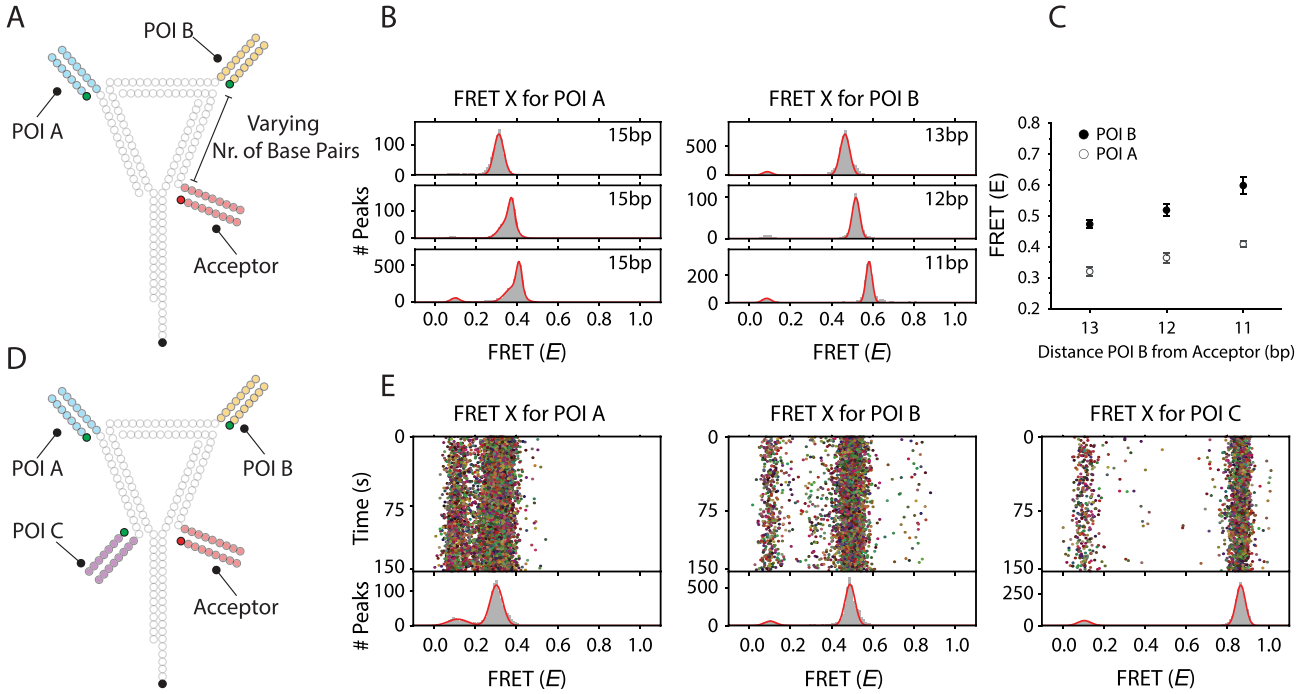

Figure 3. Structural analysis of a complex DNA nanostructure using FRET X. (A) Schematic representation of the dsDNA nanostructure used for the determination of several POIs in a single molecule. The DNA nanostructure consist of 2 POIs, one of which is fixed (POI A, blue circles) at 15-bp apart from the acceptor imager binding site. The second POI (POI B, orange circles) is separated by different linker lengths from the acceptor. The acceptor (Cy5)-labeled imager strand binds transiently to a unique binding site (red circles) to avoid photobleaching of the acceptor fluorophore. (B) FRET X histograms of the different POIs in the DNA nanostructure. For a DNA nanostructure with a 13-bp linker between POI B and the acceptor, we observe a FRET efficiency of 0.31 ± 0.01 and 0.47 ± 0.02 for POI A and POI B, respectively (Figure 3B, top row). Next, by only decreasing the linker length with steps of 1-bp between POI B and the acceptor, we observed an increase in FRET efficiency for POI B (0.52 ± 0.01 and 0.60 ± 0.02 for 12-bp and 11-bp, respectively). Furthermore, the FRET efficiency for POI A and the acceptor increases when the linker between POI B and acceptor is shorter, which hints global distortion of the nanostructure due to the shortening of one side of the triangle (left panel). (C) The mean FRET X efficiency for POI A (open circles) and POI B (solid circles) determined on different days. Mean FRET efficiencies and standard deviation are calculated from three independent experiments. (D) Schematic representation of a dsDNA nanostructure with three POIs. A third POI is added close to the acceptor binding site. (E) Kymographs obtained for each POI of the dsDNA nanostructure. In a first round of FRET X imaging, we observed a FRET efficiency of 0.27 ± 0.01 for POI A. The second round of FRET X imaging resulted in a FRET efficiency of 0.47 ± 0.02 for POI B. In a final round of FRET X imaging, we observed a FRET efficiency of 0.86 ± 0.01 for POI C in the DNA nanostructure. Mean FRET efficiencies and standard deviation are calculated from three independent experiments.

of FRET X imaging using the imager strand complementary to the POI A, we observed a single FRET peak at 0.87 reporting on the POI A (Figure 2K). As shown in Figure 2J,L, FRET X allows for the accurate detection of both POIs even when they are in closer proximity. We note that the conformation of the partially hybridized template strand is different between Figure 2 panels D,E and panels I–L due to the sequence difference of an unoccupied binding site, which consequently leads to slightly different FRET efficiencies.

Our FRET X approach allows for the detection of only a single POI for a prolonged time until another imager strand is introduced. Therefore, while each histogram showed a wide distribution of ∼0.05 (Figure 2I,J, the standard deviation) of the peak, the Gaussian fit can be used to resolve the center of a peak with high precision of <0.005 (standard error of mean), where the achievable precision depends on the number of binding events (Supplementary Figure 4A,B). The resolved FRET values for each POI are plotted as the FRET fingerprint of the measured object (Figure 2M,N).

Structural analysis of complex biomolecules using single-molecule FRET requires the detection of multiple FRET pairs in a single object. To demonstrate the potential of FRET X, we designed a DNA nanostructure consisting of two POIs and tested whether FRET X can obtain distance information for each POI in a single object. The DNA nanostructure is in a triangular shape that consists of an acceptor reference point, and a POI is placed at each corner of the triangle (Figure 3A). To avoid the photobleaching of the acceptor dye, we designed a unique sequence near the 3′ end of the construct where a complementary acceptor-labeled imager strand can transiently bind. To increase the probability of energy transfer between donor and acceptor fluorophores, the acceptor imager strand was designed to have a higher binding rate and lower dissociation rate than the donor imager strands.[21,22] We estimated the time-dependent FRET detection rates for both static and dynamic acceptor strand. The static acceptor showed a faster decrease in the FRET detection rate due to photobleaching (Supplementary Figure 6).

In a first round of FRET X, we determined the FRET efficiency for POI A that is separated by a 15-bp linker from the acceptor and observed a distinct FRET peak at 0.31 (Figure 3B, top-left panel). Next, we washed the chamber and injected the imager strand for POI B and observed a FRET peak at 0.47 when POI B is 13-bp away from the acceptor (Figure 3B, top-right panel).

To determine the resolution of FRET X for the detection of multiple POIs in a nanoscale object, we changed the length between the acceptor and POI B by a step of 1-bp. For each

https://doi.org/10.1021/acs.nanolett.1c00725
Nano Lett. 2021, 21, 3295−3301

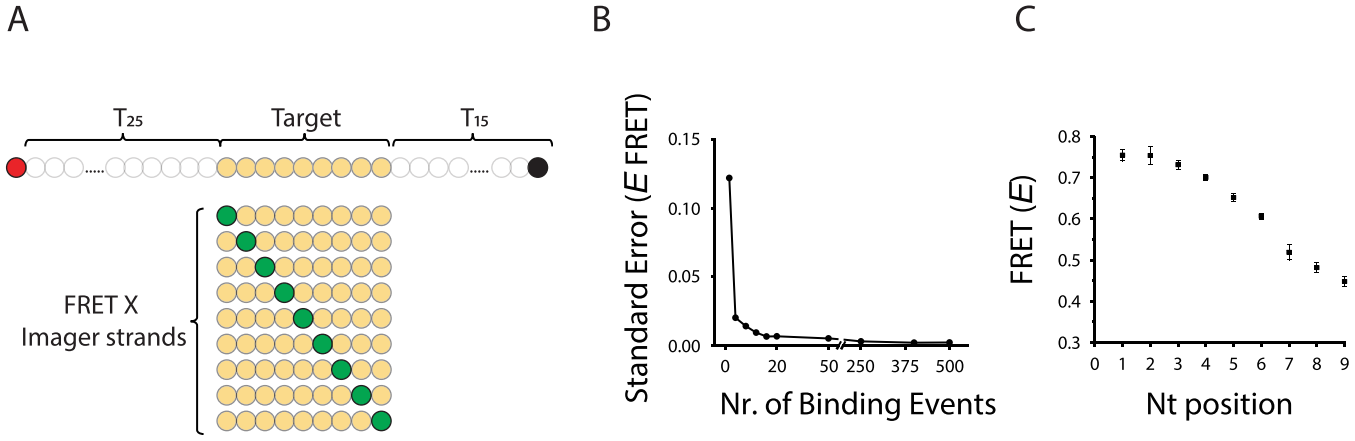

Figure 4. Single nucleotide resolution can be achieved with FRET X. (A) Schematic representation of the single-molecule constructs used for the determination of different POIs separated by a single base pair. An acceptor (Cy5, red circle) labeled ssDNA target construct consisting of a 9-nt target sequence (orange circles) where each imager strand can bind. A series of donor (Cy3, green circles) labeled FRET X imager strands. The position of each POI (or nucleotide) in the target sequence will be determined one by one using our FRET X approach. (B) Standard error of the FRET X efficiency for imager strand 5 (Supplementary Figure 5E) versus the number of binding events. We observe that we can determine the center of a Gaussian fit with a FRET X precision of $\Delta E \sim 0.01$ after >10 binding events. (C) The mean FRET X efficiency for each of the POIs determined on different days. We find good reproducibility for FRET X. Mean FRET efficiencies and standard deviation are calculated from three independent experiments.

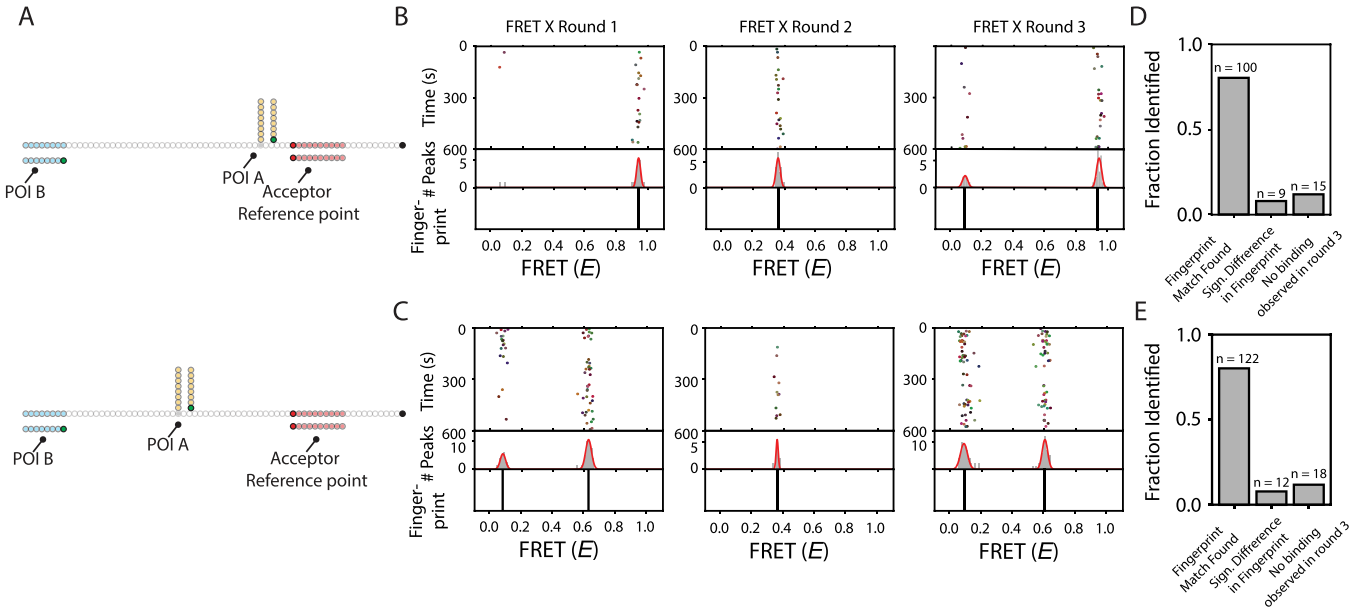

Figure 5. Population analysis on the individual molecule level using FRET X. (A) Schematic representation of the DNA constructs used for population analysis. The ssDNA construct contains two POIs, of which one is fixed and has the same location relative to the acceptor on both constructs. The second POI is connected to the side chain of one of the nucleotides in the backbone sequence and has a different location on both constructs. (B,C) Kymographs of individual molecules obtained for an equal mixture of the ssDNA constructs immobilized on the slide surface. The FRET X cycle consisted of three rounds. In a first round of the FRET X cycle, we determined the unique fingerprint of POI A among the different constructs and observe a FRET efficiency of 0.94 for the high-FRET construct panel B, left panel) and 0.63 for the medium-FRET construct (panel C, left panel). The second round of the FRET X cycle resulted in a single peak obtained from FRET between POI B and the acceptor, which is identical in both constructs (panels B,C, middle panels). In the last round of the FRET X cycle (panels B,C, right panels) we confirmed the location of POI A and observed the same FRET peaks as in round 1. (D,E) Bar plots showing the fractions of fingerprint matches and nonmatches for individual molecules that were identified as high- (panel D) or medium-FRET construct (panel E). We determined the mean FRET efficiency of the medium- or high-FRET fingerprint in round 1 and compared this with a detection uncertainty of $\Delta E \sim 0.07$ with round three to find positives matches. The majority of molecules were identified identically between round 1 and 3, for the high- (panel D) and medium- (panel E) FRET ssDNA constructs.

construct, we determined the FRET efficiency for both POIs and observed a clear change in FRET for POI B (Figure 3B, right panels, and Figure 3C, solid circles). Furthermore, the FRET efficiency for POI A and the acceptor increased when the linker between POI B and acceptor was shorter (Figure 3B, left panels, and Figure 3C, open circles).

To further demonstrate the ability of FRET X for the detection of multiple POIs, we added a third POI to the triangular DNA structure (Figure 3D). POI C was introduced

https://doi.org/10.1021/acs.nanolett.1c00725
Nano Lett. 2021, 21, 3295−3301

at a site close to the acceptor reference point and gives a high FRET value (Figure 3E, right panel). For POI A and B, we observed similar FRET efficiencies compared to their location in the structure with only two POIs (Figure 3E left and middle panels, and Figure 3B top panels).

To investigate the ultimate resolution of FRET X, we designed a series of ssDNA constructs in which the position of the donor imager binding site is altered by only a single nucleotide among the different imager strands (Figure 4A). The FRET X cycle was then repeated for all nine imager strands. The center of a peak of each histogram was determined by fitting with a single Gaussian function. The obtained fingerprint showed nine separated peaks, one for each donor-labeled nucleotide (Figure 4B and Supplementary Figure 5), indicating that FRET X has a single-nucleotide resolution.

To determine the precision that can be obtained using our FRET X approach, the standard error of the FRET efficiency was plotted as a function of the number binding events. The chosen events were from an imager strand labeled at position 5 (Supplementary Figure 5E) that yielded a FRET efficiency value of 0.65. Given our photon count rate of 5000 s^{-1} and the binding dwell time of 2 s (Supplementary Figure 1A), we expect the theoretical limit[23] of the precision in FRET determination was ∼0.005 (Supplementary Figure 4C,D). Experimentally, however, we found that the center of a Gaussian fit can be determined with a precision of $\Delta E \sim 0.01$ after obtaining >10 binding events (Figure 4B) due to other noise contributions such as electronic shot noise and backgrounds, stray light, and an uneven illumination profile. The reproducibility of FRET X was demonstrated by measuring all nine labeled imager strands on different days. As shown in Figure 4C, the standard deviation between the measurements made on different days is about 0.02 for each construct.

Finally, having the high-resolution analysis of different POIs in a nanoscopic object without photobleaching problems, we speculated that FRET X can be used reliably for population analysis at the single-molecule level, which requires repeated sampling of individual targets. To demonstrate the potential use of FRET X for population analysis at the single-molecule level, we designed two ssDNA constructs with structural differences and tested whether individual molecules can be distinguished when the two are mixed. The ssDNA constructs consist of two POIs, one of which is located at an identical position on the two DNA constructs. The second POI is connected to the side of one of the nucleotides in the backbone sequence and has a different location on the two constructs (Figure 5A and Supplementary Figures 7 and 8). To avoid the photobleaching of the acceptor dye, we designed a unique sequence near the 3′ end of the construct where a complementary acceptor labeled imager strand can transiently bind. We immobilized a mixture of the two constructs in a 1:1 ratio.

In a first round of FRET X, we determined the FRET efficiency for POI A and observed two distinct FRET populations reporting on the distinct distance between POI A and the acceptor reference point for the two different constructs (Figure 5B,C, left panels). Next, we washed the microfluidic chamber and injected the imager strand for POI B. As expected, we observed a single peak for POI B, reporting on the same position of POI B for both constructs (Figure 5B,C, middle panels). In a final round of FRET X, we confirmed the location of POI A by injecting the imager strand for POI A back and observed the same FRET peaks as in the FRET X imaging round 1 (Figure 5B,C, right panels).

For each individual molecule, we determined the mean FRET efficiency for POI A in round 1 and 3 compared this with the FRET efficiency obtained for POI A in round 3 (Supplementary Figure 9). The majority (>80%) of the individual molecules in the mixture had a similar resolved FRET efficiency of POI A between rounds 1 and 3 for the high- (Figure 5D) or medium- (Figure 5E) FRET constructs. Only a small fraction of molecules did not show a match between the FRET X rounds due to a different resolved FRET efficiency for POI A or a lack of imager strand binding events (Figure 5D and E). Altogether, these results show that the FRET X method is capable of detecting the populations of individual DNA constructs at the single-molecule level.

DISCUSSION

Here, we present a proof-of-concept for FRET X, a novel tool for the detection of several FRET pairs in a single object, which can be used for the structural analysis of biomolecules. Our FRET X technique relies on the dynamic binding of fluorescently labeled short oligos to complementary docking sequences on a target object. Conventional single-molecule FRET techniques report on the changes in distance between a single dye pair on a single molecule. In contrast, FRET X uses orthogonal imager strands for different POIs which allow us to separate the detection in time and consequently detect a large number of POIs on a single object. Both switchable FRET and FRET X use a stochastic on−off method. However, unlike switchable FRET, FRET X allows for probing one and only one location for a prolonged time until another imager strand is introduced by an operator. Therefore, we can collect higher precision data for each location. We note that our FRET X technique can be integrated with another recently developed multiplexed FRET barcode technique,[24] which allows simultaneous observation of multiple orthogonal probes, reducing the total measurement time.

Single-molecule FRET has recently been combined with super-resolution imaging using DNA-PAINT to allow for faster acquisition[21,25] and multiplexing based on FRET efficiency.[22] While FRET X is designed to report on position and distance information on different POIs in a single object, we envision that it can also be used to improve the resolution of current DNA-PAINT technologies.

ASSOCIATED CONTENT

Supporting Information

The Supporting Information is available free of charge at https://pubs.acs.org/doi/10.1021/acs.nanolett.1c00725.

Figures showing the kinetics of the FRET X imager strands, the theoretical and practical limit of FRET X, and all materials and methods including DNA sequences used for the single-molecule experiments (PDF)

AUTHOR INFORMATION

Corresponding Author

Chirlmin Joo − *Department of BioNanoScience, Kavli Institute of Nanoscience, Delft University of Technology, 2629HZ Delft, The Netherlands;* orcid.org/0000-0003-2803-0335; Email: c.joo@tudelft.nl

https://doi.org/10.1021/acs.nanolett.1c00725
Nano Lett. 2021, 21, 3295−3301

Authors

Mike Filius − *Department of BioNanoScience, Kavli Institute of Nanoscience, Delft University of Technology, 2629HZ Delft, The Netherlands*

Sung Hyun Kim − *Department of BioNanoScience, Kavli Institute of Nanoscience, Delft University of Technology, 2629HZ Delft, The Netherlands;* orcid.org/0000-0001-9272-7036

Ivo Severins − *Department of BioNanoScience, Kavli Institute of Nanoscience, Delft University of Technology, 2629HZ Delft, The Netherlands*

Complete contact information is available at: https://pubs.acs.org/10.1021/acs.nanolett.1c00725

Author Contributions

M.F. and C.J. initiated and designed the project. M.F. and S.H.K. performed the experiments. S.H.K and I.S. wrote the analysis software. M.F., S.H.K., and C.J. analyzed and discussed the data. M.F. and C.J. wrote the manuscript. All authors read and improved the manuscript.

Notes

The authors declare no competing financial interest.

■ ACKNOWLEDGMENTS

We thank Viktorija Globyte and Raman van Wee for critical reading and feedback. We thank Misha Klein for help on the analysis software. C.J. was supported by Vrije Programma (SMPS) of the Foundation for Fundamental Research on Matter and Human Frontier Science Program (RGP0026/2019).

■ REFERENCES

(1) Shi, Y. A glimpse of structural biology through X-ray crystallography. *Cell* **2014**, *159*, 995−1014.

(2) Nogales, E.; Scheres, S. H. W. Cryo-EM: A Unique Tool for the Visualization of Macromolecular Complexity. *Mol. Cell* **2015**, *58*, 677−689.

(3) Henzler-Wildman, K. A.; et al. Intrinsic motions along an enzymatic reaction trajectory. *Nature* **2007**, *450*, 838−844.

(4) Algar, W. R.; Hildebrandt, N.; Vogel, S. S.; Medintz, I. L. FRET as a biomolecular research tool — understanding its potential while avoiding pitfalls. *Nat. Methods* **2019**, *16*, 815−829.

(5) Lerner, E.; et al. Toward dynamic structural biology: Two decades of single-molecule förster resonance energy transfer. *Science (80-.).* **2018**, 359.

(6) Hohng, S.; Joo, C.; Ha, T. Single-Molecule Three-Color FRET. *Biophys. J.* **2004**, *87*, 1328−1337.

(7) Clamme, J. P.; Deniz, A. A. Three-color single-molecule fluorescence resonance energy transfer. *ChemPhysChem* **2005**, *6*, 74−77.

(8) Kalinin, S.; et al. A toolkit and benchmark study for FRET-restrained high-precision structural modeling. *Nat. Methods* **2012**, *9*, 1218−1225.

(9) Hellenkamp, B.; Wortmann, P.; Kandzia, F.; Zacharias, M.; Hugel, T. Multidomain structure and correlated dynamics determined by self-consistent FRET networks. *Nat. Methods* **2017**, *14*, 176−182.

(10) Peulen, T. O.; Opanasyuk, O.; Seidel, C. A. M. Combining Graphical and Analytical Methods with Molecular Simulations to Analyze Time-Resolved FRET Measurements of Labeled Macromolecules Accurately. *J. Phys. Chem. B* **2017**, *121*, 8211−8241.

(11) Craggs, T. D.; Kapanidis, A. N. Six steps closer to FRET-driven structural biology. *Nat. Methods* **2012**, *9*, 1157−1159.

(12) Uphoff, S.; et al. Monitoring multiple distances within a single molecule using switchable FRET. *Nat. Methods* **2010**, *7*, 831−836.

(13) Giannone, G.; et al. Dynamic superresolution imaging of endogenous proteins on living cells at ultra-high density. *Biophys. J.* **2010**, *99*, 1303−1310.

(14) Schoen, I.; Ries, J.; Klotzsch, E.; Ewers, H.; Vogel, V. Binding-activated localization microscopy of DNA l. *Nano Lett.* **2011**, *11*, 4008−4011.

(15) Sharonov, A.; Hochstrasser, R. M. Wide-field subdiffraction imaging by accumulated binding of diffusing probes. *Proc. Natl. Acad. Sci. U. S. A.* **2006**, *103*, 18911−18916.

(16) Jungmann, R. Super-Resolution Microscopy by Fluorescence Imaging of Transient Binding on DNA Origami. *Nano Lett.* **2010**, *10*, 4756−4761.

(17) Jungmann, R.; et al. Multiplexed 3D cellular super-resolution imaging with DNA-PAINT and Exchange-PAINT. *Nat. Methods* **2014**, *11*, 313−318.

(18) Dai, M.; Jungmann, R.; Yin, P. Optical imaging of individual biomolecules in densely packed clusters. *Nat. Nanotechnol.* **2016**, *11*, 798−807.

(19) Schnitzbauer, J.; Strauss, M. T.; Schlichthaerle, T.; Schueder, F.; Jungmann, R. Super-resolution microscopy with DNA-PAINT. *Nat. Protoc.* **2017**, *12*, 1198−1228.

(20) Filius, M.; et al. High-Speed Super-Resolution Imaging Using Protein-Assisted DNA-PAINT. *Nano Lett.* **2020**, *20*, 2264−2270.

(21) Auer, A.; Strauss, M. T.; Schlichthaerle, T.; Jungmann, R. Fast, Background-Free DNA-PAINT Imaging Using FRET-Based Probes. *Nano Lett.* **2017**, *17*, 6428−6434.

(22) Deußner-Helfmann, N. S.; et al. Correlative Single-Molecule FRET and DNA-PAINT Imaging. *Nano Lett.* **2018**, *18*, 4626−4630.

(23) Holden, S. J.; et al. Defining the limits of single-molecule FRET resolution in TIRF microscopy. *Biophys. J.* **2010**, *99*, 3102−3111.

(24) Kim, S. H.; Kim, H.; Jeong, H.; Yoon, T.-Y. Encoding Multiple Virtual Signals in DNA Barcodes with Single-Molecule FRET. *Nano Lett.* **2021**, *21*, 1694−1701.

(25) Lee, J.; Park, S.; Hohng, S. Accelerated FRET-PAINT microscopy. *Mol. Brain* **2018**, *11*, 70.